

Experimental and Numerical Correlation of Impact of Spherical Projectile for Damage Analysis of Aero Engine Component

Anuradha Nayak Majila*, Rajeev Jain, Chandru Fernando D., and S. Ramachandra

Gas Turbine Research Establishment, Bengaluru - 560 093, India

**E-mail: nayakmajila.anuradha@gmail.com*

ABSTRACT

Studies the impact response of flat Titanium alloy plate against spherical projectile for damage analysis of aero engine components using experimental and finite element techniques. Compressed gas gun has been used to impart speed to spherical projectile at various impact velocities for damage studies. Crater dimensions (diameter and depth) obtained due to impact have been compared with finite element results using commercially available explicit finite element method code LS-DYNA. Strain hardening, high strain rate and thermal softening effect along with damage parameters have been considered using modified Johnson-Cook material model of LS-DYNA. Metallographic analysis has been performed on the indented specimen. This analysis is useful to study failure analysis of gas turbine engine components subjected to domestic object damage of gas turbine engine.

Keywords: Domestic object damage, metallographic, FEM, LS-DYNA, spherical projectile

1. INTRODUCTION

The impact of two bodies is highly complicated phenomenon. The major characteristics are the short duration and large magnitude of the contact forces generated during the impact event. This phenomenon is associated with stress wave's propagation through the bodies and associated localised deformation. Domestic object damage (DOD) is the damage caused due to impact of the inner components (loose bolts, nuts and washer) of the engine with its main components (rotating and static blades, inlet-strut, casings, etc.) during engine operating condition. In these events velocity of the projectile generally varies from 40 m/s - 100 m/s.

Hertz¹ pioneered the classical contact problem of two colliding bodies for elastic and elastic-plastic materials. A comprehensive reference of contact problems of spherical bodies can be found in the classical works of Timoshenko and Goodier². Further sources of references on indentation and allied subjects are given by Goldsmith³ and Johnson⁴, and contact mechanic book by Johnson⁵.

With the advent of computer technology experimental testing on impact event is getting replaced with numerical simulation. Experimental and computational work in impact studies is getting enormous attention for understanding fundamental principles of impact phenomena. Modern explicit FEM numerical codes such as LS-DYNA have the capabilities of including non-linear material properties with strain-hardening and strain-rate dependent material effects for impact studies. Extensive work has been done to understand foreign object damage (FOD) behaviour of aero engine components. Hong⁶, *et al.* evaluated residual stresses in a three dimensional objects using FEM and studied the effect of initial yield stress,

impact velocity, diameter of projectile and incident angle of impact. Meguid^{7,8} examined the effect of projectile and target parameters upon the deformed zone and induced residual stresses using DYNA-3D FEM code. Experiments indicate that FOD on rotor blades produce indentation having size of the order of milli-meter with impact velocities varying from 200 m/s – 350 m/s, depending on the blade speed of a specific engine⁹⁻¹¹. Although it is possible to assess residual stress, stress concentration factor and crater geometry using finite element technique but experimental validation of these results are crucial for various means.

Study carried out by Mall¹², *et al.* shows that impact phenomenon changes the micro-structure of material. Peters and Ritchie¹³ studied the effect of microstructure in titanium material due to FOD and later Peters¹⁴, *et al.* used Kitagawa-Takahashi approach to evaluate high cycle fatigue limit of a component subjected to FOD. A similar kind of approach has been suggested by Nowell^{15,16}, *et al.*

This paper studies the impact response of spherical projectile on titanium plate in the velocity range varying from 50 m/s to 95 m/s using experimental and finite element techniques. Strain hardening, high strain rate and thermal softening effects have been included in the FEM analysis using Johnson-Cook material model. Crater diameter and residual growth obtained through experimental studies have been correlated with numerical results at different impact velocities. Metallographic study has been done to obtain microstructure and hardness in the vicinity of impact.

2. EXPERIMENTAL SETUP

Impact of spherical projectile on titanium specimen was

conducted at room temperature using a compressed air gun shown in Fig. 1. This test facility has a capacity to launch spherical projectile up to a speed of 150 m/s depending on the mass of the projectile. It is equipped with high speed camera which can capture images at the rate of 1,00,000 frames per second.



Figure 1. Compressed air gun test setup.

In this arrangement spherical projectile of 35 mm diameter and a mass of 0.16 kg and having Rockwell hardness of 62 RC is inserted in a long barrel. Compressed air is used to fill the gas reservoir to a specific level of pressure depending on the velocity of the projectile. Thereafter, the valve is opened instantaneously to accelerate the projectile through the air gun.

Flat titanium (Ti-6Al-4V) plates of length, width and thickness 450 mm, 250 mm, and 5 mm respectively as shown in Fig. 2 has been used as a target plate to study impact response of spherical projectile at the centre of the plate. This plate is clamped at the free ends, inside the enclosed chamber using rigid steel blocks to cater the safety of the person witnessing

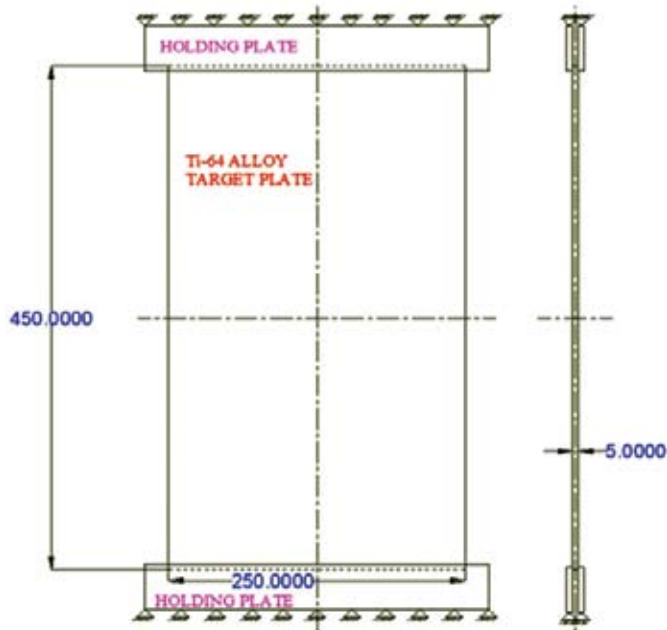


Figure 2. Geometric model of flat plate.

the test. Figure 3 shows micro-structure of this plate along rolling and impact directions. This figure indicates that present alloy is having equiaxed primary α on inter-granular β matrix. Average Vickers Micro-Hardness (VHN) of titanium material consider for investigation along rolling direction is 297 VHN.

Five tests were conducted by varying air reservoir pressure to achieve five different impact velocities varying from 53 m/s, 64 m/s, 75 m/s, 81 m/s, and 95 m/s. Incident and rebound velocities of the projectile were measured by analyzing the recorded video file of each impact event using high speed motion analysis software.

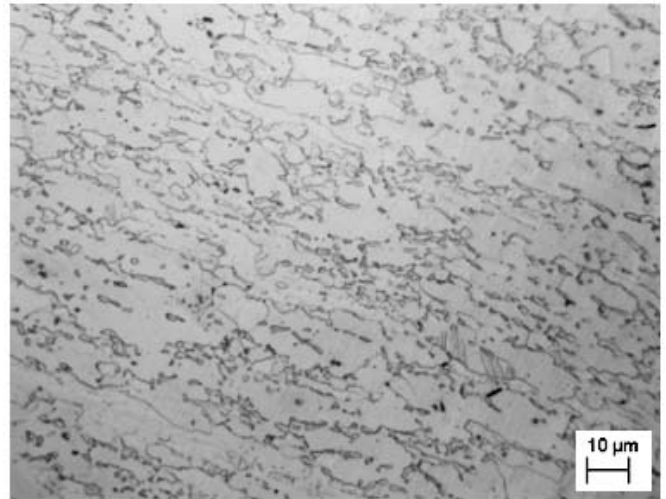


Figure 3. Microstructure of the plate along rolling and impact directions.

3-D scanning machine was used to measure residual deformation (post impact) and this includes crater diameter and depth using indicator probe. Indicator probe was freely moved on the impacted surface of the target plate to obtain depth and diameter of the crater.

Metallurgical behaviour of impacted specimen was studied by cutting the plate along the centre of the plate using EDM machine. After that, the cross-sectioned plates (without polishing) were studied under stereo-microscope at low resolution. This study shows localised cup formation and indicates the path of shear crack propagation (as shown in Fig. 8).

After stereo-microscopic study the specimens were polished and etched using standard Kroll solution to reveal the metallurgical structure under optical microscope. Micro-hardness measurement on the half-sectioned specimens, across the thickness of the target, across localised shear bands & near the contact area of impact were taken to study any hardness related change due to impact by using Vickers Micro-Hardness equipment.

3. DIMENSIONAL ANALYSIS

Figure shows elastic spherical projectile impacting normal to the surface of Ti-6Al-4V plate at its centre. This plate is supported rigidly in between two steel rigid blocks.

Initial kinetic energy of the spherical projectile is given as

$$KE = \frac{\pi}{12} D_p^3 \rho_p V_0^2 \quad (1)$$

where ρ_p is the projectile density; D_p is the diameter of the projectile and V_0 is the impact velocity of the projectile.

Work done in expanding the hole of target plate is

$$W = \frac{\pi}{2} \sigma_y D_p^2 h \quad (2)$$

where σ_y is the yield stress of the target plate; h is the thickness of the target plate.

Dividing Eqn. (1) by Eqn. (2) non-dimensional impact energy can be given as

$$\Omega_n = \frac{\rho_p D_p}{6 \sigma_y h} V_0^2 \quad (3)$$

Later, Taylor and Thomson as referred in the book by Zukas¹⁷, gave solution to obtain workdone in stretching and bending of the elements of the plane and increasing the radius during dishing. According to this theory workdone is expressed as

$$W = \frac{\pi}{2} D_p \sigma_y h (D_p + \pi h) \quad (4)$$

This equation reveals that there are two types of energy in bending phenomena i.e. stretching energy as given in Eqn. (2) and bending energy. Dishing is favourable when thickness of the plate is lesser than diameter of the spherical projectile. In case of thin plate bending and stretching is more favourable than expansion of hole in radial direction. Bending resistance increases with increase in plate thickness by square of thickness and dishing becomes unfavourable.

4. FINITE ELEMENT MODEL

Impact response of spherical projectile on Ti-6Al-4V specimen has been done using explicit finite element solver LS-DYNA. The time increments in the explicit analysis should be lesser than the time required for an elastic wave to traverse the smallest element. Local heating and its flow stress and fracture strain has been included using modified Johnson-Cook material model of LS-DYNA software.

4.1 Finite Element Mesh

Finite element model of Ti-6Al-4V specimen with clamped ends and spherical projectile is generated using three dimensional 8-node linear brick elements. Figure 4 shows finite element mesh model of Ti-6Al-4V specimen with spherical projectile. This figure also indicates mesh in the vicinity of contact region. Sufficiently very fine and uniform brick mesh of the dimension of 0.35 mm x 0.3 mm x 0.3 mm has been used near contact region. Surface to surface contact with penalty contact formulation is used for defining the contact between plate and the sphere. In order to save computer time symmetrical boundary condition has been used across the centre plane of symmetry.

All the quality parameters of each element have been checked and maintained at highest quality level for the highest accuracy of the results. Finite element model of flat plate consists of 272507 nodes and 256700 solid brick elements using reduce integrated elements of explicit finite element solver

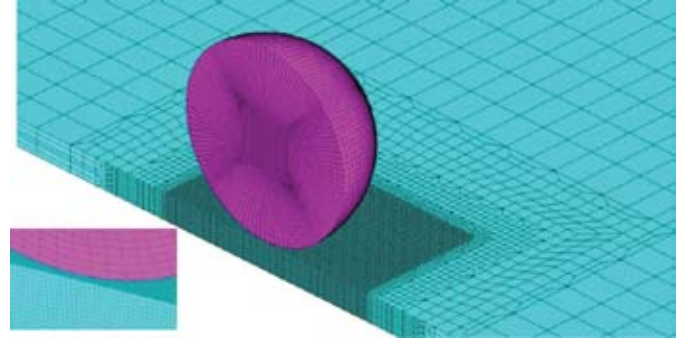


Figure 4. Symmetrical model of titanium specimen with spherical projectile.

LS-DYNA. Similarly, spherical projectile has been modelled using eight node solid brick elements using reduce integration method. This spherical ball model consists of 114688 nodes and 118877 elements.

4.2 Material Model

Perforation of Ti-6Al-4V plate is studied using Johnson-Cook (J-C) material model and explicit finite element code LS-DYNA. Modified J-C material model for Ti-6Al-4V plate¹⁸ has been considered to simulate the impact response of elastic spherical steel projectile on specimen.

4.2.1 Ti-6Al-4V plate

Modified J-C material model considers the effect of strain hardening, strain-rate and thermal softening effects of the material during impact event. This material model has been modified in the numerical code to predict better results (Dey¹⁹, *et al.*). In this modified version equivalent stress as a function of strain hardening, strain rate and temperature is given as

$$\sigma_{eq} = (A + B \varepsilon_{eq}^n) (1 + (\dot{\varepsilon}_{eq} / \dot{\varepsilon}_0)^c) (1 - T^{*M}) \quad (5)$$

where A , B , C , and M are material constants; n is the strain hardening exponent; $\dot{\varepsilon}_{eq}$ is the equivalent plastic strain rate and is reference strain rate; T is the homologues temperature defined as $T^* = (T - T_{room}) / (T_{Melt} - T_{room})$ where T_{Melt} and T_{room} is the melting and room temperature of the material respectively.

A fracture criterion of Ti-6Al-4V plate is simulated on the basis of void growth proposed by Rice and Tracey²⁰. This criterion is based on the growth of an initially spherical void in a perfect plastic material. Hancock and Mackenzie²¹ extended this criteria and showed mathematically that fracture strain is given as

$$\varepsilon_f = \varepsilon_n + \frac{1}{0.283} \log \left(\frac{R}{R_0} \right) \exp \left(-\frac{3}{2} \frac{\sigma_H}{\sigma_{eq}} \right) \quad (6)$$

Several studies show that failure strain increases with increase in temperature and decreases with increase in strain rate. Johnson-Cook extended this criterion by including strain rate and thermal softening effect in Eqn. (6) and concluded that failure strain can be predicted as

$$\varepsilon_f = (D_1 + D_2 \exp(-D_3 \sigma^*)) (1 + (\dot{\varepsilon}_{eq} / \dot{\varepsilon}_0))^{D_4} (1 + D_5 T^*) \quad (7)$$

where $D_1 \dots D_5$ are damage parameters of material; $\dot{\varepsilon}_{eq}$ is strain rate and $\dot{\varepsilon}_0$ is users defined reference strain rate; $\sigma^* = \sigma_H / \sigma_{eq}$

is the stress-triaxiality ratio defined as ratio of hydrostatic stress (σ_H) to the equivalent stress (σ_{eq}). Thus failure of this material model takes into consideration the effect of stress triaxiality, strain hardening and thermal softening of the material.

The evolution of damage D is given by the accumulated incremental effective plastic strains divided by the current strain at fracture. The fracture criterion is based on damage evolution, where the damage D of a material element is expressed as

$$D = \sum \frac{\Delta \epsilon_{eq}}{\epsilon_f} \quad (8)$$

$\Delta \epsilon_{eq}$ is the increment of the accumulated equivalent plastic strain that occurs during an integration cycle. Failure is assumed to occur when D equals to unity. Material parameters of this material model are shown in Table 1.

Table 1 Material parameters of Ti-6Al-4V

Material parameters		Damage parameters	
Material properties	Value	Damage constant	
Density	4428 kg/m ³	D_1	-0.09
Young's modulus	116 GPa	D_2	0.27
Poisson's ratio	0.31 γ	D_3	0.48
yield stress (A)	1098 (MPa)	D_4	0.014
hardening coefficient (B)	1092 (MPa)	D_5	3.87
strain hardening exponent	0.93 n		
strain rate constant (C)	0.014		
softening exponent (M)	1.1		
Melting temperature T_m	1878 K		
Specific heat C_p	560 J/kg °C		

4.2.2 Spherical Projectile

Details of material properties of spherical steel projectile is provided in Table 2.

Table 2. Material properties of steel

Material Property	Properties Values
Elastic modulus (E)	204 GPa
Poisson's ratio (ν)	0.33
Mass density (ρ)	7952 kg/m ³

5. RESULTS AND DISCUSSION

Present results compare finite element and test results. Thereafter, microstructure study has been carried out to identify shear band, mode of failure and material hardness near impact region.

5.1 Kinetic Energy of Projectile and Plate

Figure 5 shows variation of kinetic energy of projectile normalised with work done to expand the hole diameter to projectile diameter at different impact velocities. Kinetic energy of spherical projectile of mass 0.18 kg ($0.5 \text{ m}v^2$) varies from 253 J to 590 J due to variation in initial velocity from 53 m/s to 81 m/s. This figure indicates that kinetic energy of target specimen increases around 50 per cent for all the cases considered in this investigation.

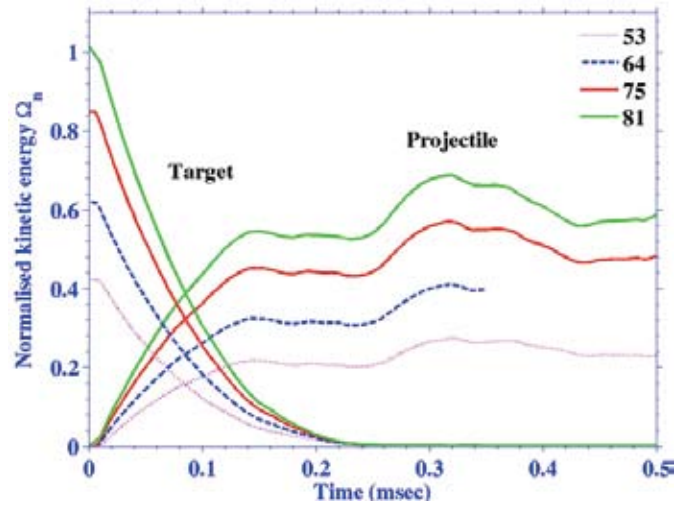


Figure 5. Temporal variation in normalised kinetic energy of projectile and target at different impact velocities.

5.2 Experimental and Numerical Correlation

Experiment test results have been compared with FEM results for four different velocities. Thereafter, crack formation in the test specimen has been studied with numerical results.

5.2.1 Crater Diameter

Figure 6 shows comparison of normalised crater diameter with experimental results at different impact velocities of spherical projectile. This figure indicates that size of crater diameter in the plate increases with increase in impact velocity of the projectile. This figure further reveals that there is a correlation in both experimental and numerical results.

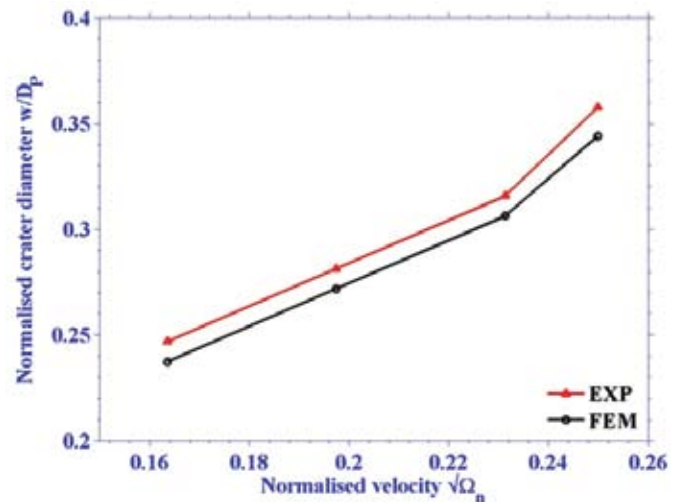


Figure 6. Variation of crater diameter with impact velocity.

5.2.2 Residual Deformation

Comparison of normalised residual depth with experimental results has been shown at various impact velocities in Fig. 7. This figure indicates that residual depth increases with increase in impact velocity and also shows excellent correlation between finite element and experimental results. These results have been tabulated (as shown in Table 3) for comparison. Table 3 indicates that maximum difference in experimental and finite element result for residual growth is

of the order of 7 per cent whereas variation in crater diameter is around 3 per cent to 4 per cent for all the impact velocities considered in this investigation.

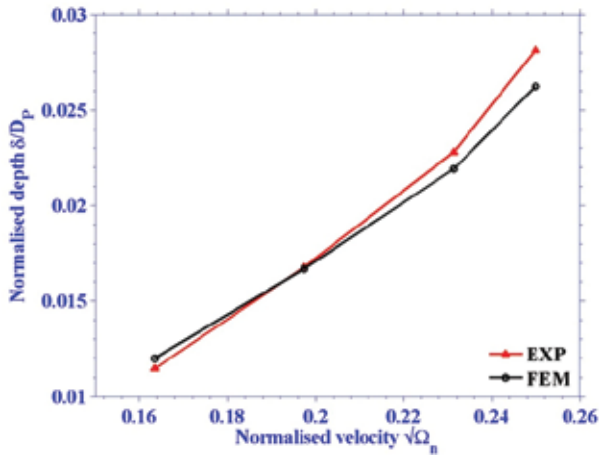


Figure 7. Variation of residual depth with impact velocity.

Table 3. Comparison of experimental and FEM results

Projectile velocity (m/s)	Crater depth (mm)			Crater diameter (mm)		
	Exp	FEM	Variation (per cent)	Exp	FEM	Variation (per cent)
53	0.4008	0.420	4.74	8.643	8.304	3.92
64	0.586	0.584	0.34	9.849	9.515	3.40
75	0.798	0.767	3.9	11.055	10.721	3.02
81	0.985	0.919	6.7	12.521	12.039	3.85

5.3 Metallographic and Numerical Study

Spherical impact on Ti-6Al-4V plate gives rise to permanent crater at the point of impact due to plastic deformation of the material. Figure 8 show the comparison between experimental results and numerical analysis of crater and crack formation at four different velocities. Deformation pattern of crater in the plate was measured at four different impact velocities by cutting the plate at the centre in longitudinal direction and thereafter stereo zoom microscope has been used for identifying the existence of cracks due to impact.

Experimental and numerical study reveals that there is no crack at impact velocity 53 m/s to 64 m/s as shown in Fig. 8(a) and Fig. 8(b). Crack appeared around contact point of spherical projectile and test specimen at projectile speed of 75 m/s as indicated in Fig. 8 (c). However, with increase in velocity, through thickness cracks started appearing as shown in Fig. 8 (c). At 95 m/s impact velocity the crater formed a plug as indicated in Fig. 9.

5.4 Microstructure

Microstructure of cross section of impacted plate as indicated in Fig. 8 (a) and Fig. 8 (b) was minutely observed

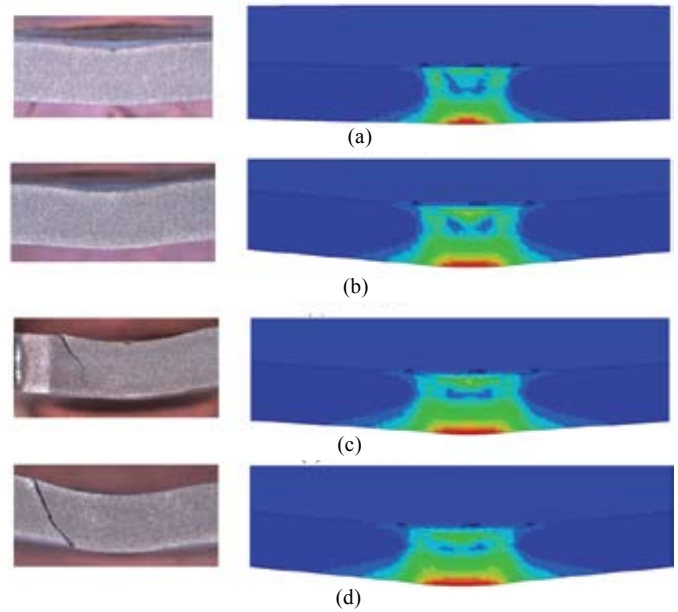


Figure 8. Experimental and FEM comparison of crater at various speeds. (a) 53 m/s, (b) 64 m/s, (c) 75 m/s, and (d) 81 m/s.



Figure 9. Experimental and FEM comparison of crater at 95 m/s; (a) Rear view and (b) Through thickness cut section.

under optical microscope with 200 X magnification. It is observed that at low velocity i.e. 53 m/s and 64 m/s the plate did not undergo any localised micro-structural changes in the vicinity of impact. With the increase in impact velocity the shear localisation is active as can be revealed from the Fig. 10. Initiation of shear band takes place when thermal softening is superseding the strain rate hardening. Beyond 75 m/s the incremental shear deformation takes place which are responsible for progressive damage in the target plate without increase in the crater depth.

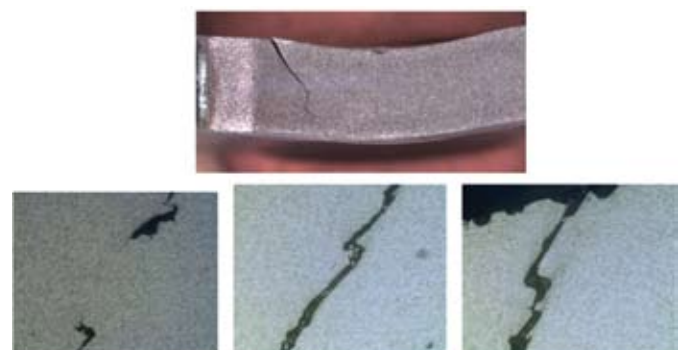


Figure 10. Deformation by shear band formation at velocity 75 m/s.

Figure 11 shows microstructure beneath the crater surface for 64 m/s impact velocity. This figure reveals that grains are more compressed in comparison with original grain size shown in Fig. 3 and further illustrates that impact indentation create deformed zone around the crater. This leads to accumulation of dislocations around the deformation zone.

Micro hardness at different depth has been observed using Vicker's-Micro-Hardness instrument. This figure illustrates that micro-hardness increases with distance reaches maximum and thereafter decreases with depth indicating that hardness is more near to indentation zone.

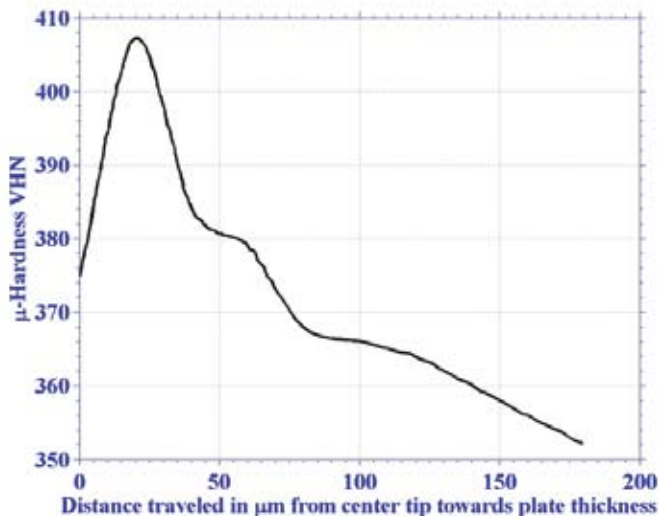
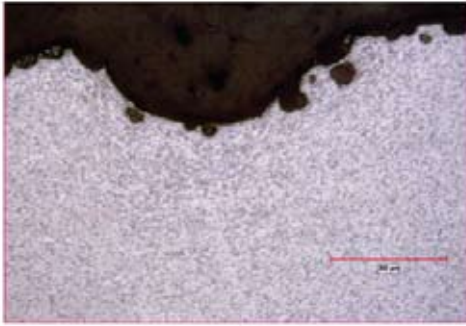


Figure 11. Optical micrographs of crater centre and micro-hardness profile, at the point of impact at 64 m/s impact velocity.

6. CONCLUSION

Experimental and finite element studies show that crater diameter and residual growth increases with increase in projectile velocity and these results are comparable for all the velocities considered in this investigation. These results further reveal that at an impact velocity of 75 m/s macro-cracks get generated circumferentially in the plate. These cracks increases with increase in impact velocity and leads to plug formation at 91 m/s projectile velocity.

REFERENCES

- Hertz, H. Uber die Berührung fester elastischer Körper. *J. Reine Angewandte Math.*, 1882, **92**, 156-71. doi: 10.1515/crll.1882.92.156
- Timoshenko, S. & Goodier, N. Theory of elasticity. McGraw-Hil, New York, 1970.
- Goldsmith, W. Impact the theory and physical behaviour of colliding solids, Edward Arnold, London, 1960.
- Johnson, W. Impact strength of materials. Edward Arnold, London, 1972.
- Johnson, K. L. Contact mechanics, Cambridge University Press, Cambridge, 1985. doi: 10.1017/CBO9781139171731
- Hong, T.; Ooi, J. Y. & Shaw, B.A. A Numerical study of the residual stress pattern from single shot impacting on a metallic component. *Adv. Eng. Software.*, 2008, **39**(9), 743-756. doi: 10.1016/j.advengsoft.2007.10.002
- Meguid, S.A.; Shagal, G.; Stranart, J.C. & Daly, J. Three-dimensional dynamic finite element analysis of shot-peening induced residual stresses induced residual stresses. *Finite Elements Anal. Design.*, 1999, **31**(3), 179-91. doi: 10.1016/S0168-874X(98)00057-2
- Meguid, S. A. Shagal, G. & Stranart, J. C. Finite element modelling of shot-peening residual stresses. *Mater. Process.*, 1999, **92-93**, 401-404. doi: 10.1016/S0924-0136(99)00153-3
- Ritchie, R. O. Boyce, B. L. Campbell, J. P. Roder, O. & Thomps. Thresholds for high-cycle fatigue in a turbine engine Ti-6Al-4V alloy. *Int. J. Fatigue.*, 1999, **21**(7) 653-662. doi: 10.1016/s0142-1123(99)00024-9
- Ritchie, R. O. Davidson, D. L. Boyce, B. L. Campbell, J. P. & Roder, O. High cycle fatigue of Ti-6Al-4V. *Fatigue Fract. Eng. Mater. Struct.*, 1999, **22**(7) 621-631. doi: 10.1046/j.1460-2695.1999.00194.x
- Jain, R. Foreign object damage analysis of leading edge of fan rotor blade. *In Proceedings of Indian National Science Academy*, 2013.
- Mall, S.; Hamrick II, J.L. & Nicholas, T. High cycle fatigue behavior of Ti-6Al-4V with simulated foreign object damage. *Mech. Mater.*, **33**(11), 679-692. doi: 10.1016/S0167-6636(01)00084-9
- Peters, J.O. & Ritchie, R.O. Foreign-object damage and high-cycle fatigue: Role of microstructure in Ti-6Al-4V. *Int. J. Fatigue*, 2001, **23**(1), 413-421. doi: 10.1016/S0142-1123(01)00168-2
- Peters, J.O.; Boyce, B.L.; Chen, X.; McNaney, J. M.; Hutchinso, J. W. & Ritchie, R.O. On the application of the Kitagawa-Takahashi diagram to foreign-object damage and high cycle fatigue. *Eng. Fract. Mech.*, 2002, **69**(13), 1425-1446. doi: 10.1016/S0013-7944(01)00152-7
- Nowell, D.; Dini, D. & Duo, P. Stress analysis of V-notches with and without cracks, with application to foreign object damage. *J. Strain Anal.*, 2003, **38**(5), 429-441. doi: 10.1243/03093240360713487
- Nowell, D.; Duo, P. & Stewart, I.F. Prediction of fatigue performance in gas turbine blades after foreign object damage. *Int. J. Fatigue.*, 2003, **25**(9-11), 963-969. doi: 10.1016/S0142-1123(03)00160-9

17. Zukas, J.A. High velocity impact dynamics. John Wiley & Sons, Inc., New York, 1990.
18. Johnson, G.R. & Cook, W.H. Fracture characteristics of three metals subjected to various strains, strain rates temperature and pressures. *Eng. Fract. Mech.*, 1985, **21**(1), 31-48.
doi: 10.1016/0013-7944(85)90052-9
19. Dey, S.; Borvik, T.; Hopperstad, O.S. & Langseth, M. On the influence of fracture criterion in projectile impact of steel plates. *Comput. Mater. Sci.*, 2006, **38**(1), 176-191.
doi: 10.1016/j.commatsci.2006.02.003
20. Rice, J. R. & Tracey, D.M. On the ductile enlargement of voids in triaxial stress fields. *J. Mech. Phy. Solids.*, 1969, **17**(3), 210-217. doi: 10.1016/0022-5096(69)90033-7
21. Hancock, J.W. & Mackenzie, A.C. On the mechanisms of ductile failure in high-strength steels subjected to multi-axial stress-states. *J. Mech. Phy. Solids.*, 1976, **24**(2-3), 147-169.
doi: 10.1016/0022-5096(76)90024-7

ACKNOWLEDGEMENT

Authors express their sincere thanks to Director GTRE for the support to carry out all experimental and analytical work. Authors express their sincere thanks to Mr Rajappa Banger for giving technical support in conducting tests and handling instruments during the tests.

CONTRIBUTORS

Ms Anuradha Nayak Majila received her BTech (Metallurgical Engineering) from NIT-Durgapur, in 2001. Presently working as Scientist 'E' at Gas Turbine Research Establishment, Bengaluru. She worked for several projects for ADA, CABS, HAL, NAL, Delhi-Metro rail and Honey well Tech Ltd. Her area of interest include: High strain rate testing, impact testing, foreign object damage evaluation of aero engine and aircraft components.

Dr Rajeev Jain received his MSc (Engg) and PhD from Indian Institute of Science, Bengaluru. Presently working as Scientist Sc 'G' and heading the group of impact mechanics at Gas Turbine Research Establishment, Bengaluru. He worked in design of safety critical gas turbine engine components. He has a vast experience in field of non-linear finite element modeling pertaining to impact, contact, composite and wave mechanics.

Mr Chandru Fernando D. completing his BE (Metallurgical Engineering). He is presently working as Scientist 'E' at Gas Turbine Research Establishment, Bengaluru. He is working in the area of material testing, data analysis and evaluation of aero engine materials. He is a life member of AeSI, IIM.

Dr S. Ramachandra currently working as Scientist G and Technical Director of Systems Engineering Group at Gas Turbine Research Establishment, Bengaluru. He worked in the field of Structural analysis and testing of aero engine components. His other fields of activities include engine casing containment testing and analysis, design and development of advanced high temperature polymer matrix composite and ceramic matrix composite components for aero engines.